

Comparison of beamformer and ICA for dynamic connectivity analysis: A simultaneous MEG-SEEG study

Stefania Coelli^a, Samuel Medina Villalon^{b,c}, Francesca Bonini^{b,c}, Jayabal Velmurugan^b, Víctor J. López-Madrona^b, Romain Carron^{b,d}, Fabrice Bartolomei^{b,c}, Jean-Michel Badier^b, Christian-G. Bénar^{b,*}

^a Department of Electronics, Information and Bioengineering, Politecnico di Milano, Milano, Italy

^b Aix Marseille University, INSERM, INS, Inst Neurosci Syst, Marseille, France

^c APHM, Timone Hospital, Epileptology and Cerebral Rhythmology, Marseille, France

^d APHM, Timone Hospital, Functional and Stereotactic Neurosurgery, Marseille, France

ARTICLE INFO

Keywords:

MEG
ICA
Beamformer
Brain connectivity
Simultaneous recordings
Source reconstruction
Epileptic network

ABSTRACT

Magnetoencephalography (MEG) is a powerful tool for estimating brain connectivity with both good spatial and temporal resolution. It is particularly helpful in epilepsy to characterize non-invasively the epileptic networks. However, using MEG to map brain networks requires solving a difficult inverse problem that introduces uncertainty in the activity localization and connectivity measures. Our goal here was to compare independent component analysis (ICA) followed by dipole source localization and the linearly constrained minimum-variance beamformer (LCMV-BF) for characterizing regions with interictal epileptic activity and their dynamic connectivity. After a simulation study, we compared ICA and LCMV-BF results with intracerebral EEG (stereotaxic EEG, SEEG) recorded simultaneously in 8 epileptic patients, which provide a unique ‘ground truth’ to which non-invasive results can be confronted. We compared the signal time courses extracted applying ICA and LCMV-BF on MEG data to that of SEEG, both for the actual signals and the dynamic connectivity computed using cross-correlation (evolution of links in time).

With our simulations, we illustrated the different effect of the temporal and spatial correlation among sources on the two methods. While ICA was more affected by the temporal correlation but robust against spatial configurations, LCMV-BF showed opposite behavior. Moreover, ICA seems more suited to retrieve the simulated networks.

In case of real patient data, good MEG/SEEG correlation and good localization were obtained in 6 out of 8 patients. In 4 of them ICA had the best performance (higher correlation, lower localization distance). In terms of dynamic connectivity, the evolution in time of the cross-correlation links could be retrieved in 5 patients out of 6, however, with more variable results in terms of correlation and distance. In two patients LCMV-BF had better results than ICA. In one patient the two methods showed equally good outcomes, and in the remaining two patients ICA performed best.

In conclusion, our results obtained by exploiting simultaneous MEG/SEEG recordings suggest that ICA and LCMV-BF have complementary qualities for retrieving the dynamics of interictal sources and their network interactions.

1. Introduction

Magnetoencephalography (MEG) is a non-invasive neurophysiological tool that records the (tiny) magnetic fields produced by neurons. It has proven to be useful both in fundamental research and in clinical practice (Bailet, 2017). An application of choice is in presurgical evaluation of drug-resistant partial epilepsy, where it can be used to map the

brain regions producing interictal epileptic discharges recorded on the surface (Jmail et al., 2016; Lin et al., 2003; Malinowska et al., 2014).

The classical analysis of MEG consists of performing source localization on interictal epileptiform discharges (IEDs) or ‘epileptic spikes’, which are more abundant than seizures and more likely to be captured in non-invasive recording with electroencephalography (EEG) and MEG. Dipole localization of IED, for example, is a commonly used method to

* Corresponding author.

E-mail address: christian.benar@univ-amu.fr (Christian-G. Bénar).

<https://doi.org/10.1016/j.neuroimage.2022.119806>.

Received 6 July 2022; Received in revised form 25 October 2022; Accepted 9 December 2022

Available online 10 December 2022.

1053-8119/© 2022 Published by Elsevier Inc. This is an open access article under the CC BY-NC-ND license (<http://creativecommons.org/licenses/by-nc-nd/4.0/>)

identify the cortical areas that may be involved in interictal discharge (Lin et al., 2003), but this approach presents several drawbacks. In particular, spikes should be detected at the M/EEG sensors level and clustered prior to localization, to obtain a reliable result (Kobayashi et al., 1999; Lin et al., 2003; Merlet and Gotman, 1999). An averaging step may also be necessary to improve the signal-to-noise ratio (SNR), and a dipole may be fitted to each averaged spike. Unfortunately, this approach prevents the characterization of the temporal dynamic of the IED events. Indeed, since epilepsy is mainly a disease of brain networks (Bartolomei et al., 2017), MEG should be able to define, in a non-invasively way, the spatio-temporal organization of such networks.

In order to improve the non-invasive analysis of interictal activities, different techniques of brain source separation and localization have been explored to extract the spatio-temporal dynamics of the underlying network in M/EEG (Hall et al., 2018; Hassan et al., 2017; Li et al., 2021; Malinowska et al., 2014; Wilenius et al., 2020). In 1999, Kobayashi (Kobayashi et al., 1999) proposed for the first time the use of the independent component analysis (ICA) to separate the interictal components from the background EEG activity and applied the dipole source modeling approach without the need for averaging. The possibility of also recovering the propagation of the IED from one component to the others was shown. This result was further validated (Kobayashi et al., 2002, 2001) by comparing the extracted epileptiform component to spike dipole localization and SEEG signals. In particular, the authors pointed out two main advantages of ICA in this context: the preservation of the individual spike waveform, which may be lost in the averaging, and the ‘objectivity’ of spike component separation. In fact, the fixed spatial field of the component can be used to fit the dipole source instead of modeling a dipole for each spike (or cluster of spikes). ICA was also applied to MEG data to improve the automatic detection of spikes, which were subsequently localized (Ossadtchi et al., 2004). More recently, a fractional type of blind source separation was introduced to extract with high accuracy the ‘dominant’ component associated to IED, generated by a unique epileptogenic zone, in multichannel MEG data (Matsubara et al., 2020).

Using simultaneous intracerebral (SEEG) and MEG recordings, Pizzo and colleagues proved that ICA can disentangle the activity of deep networks from that of neocortical structures, further supporting the possibility to separate the different epileptic sources as independent components and then localize them (Pizzo et al., 2019). To complement epilepsy research, a similar approach (second order blind identification) was used by López-madrona and colleagues to identify correspondences between MEG and SEEG activities from mesial brain networks related to cognitive processes (López-Madrona et al., 2022).

However, the possibility that interictal activity detected at the scalp surface may involve multiple sources has been rarely explored with this approach. Malinowska used ICA on MEG alone in order to extract spiking components and recover interictal propagation network in MEG signals of epileptic patients (Malinowska et al., 2014). The propagation network was obtained by exploiting the spike co-occurrences and delays on multiple ICs, showing a significant overlap to the epileptic network as identified by analyzing SEEG recordings.

Another popular approach to investigate the interictal activity in epilepsy, is based on spatial filtering or “beamformer”, which is widely applied for reconstructing the time courses at specific brain locations. One example is the linearly constrained minimum-variance beamformer (LCMV-BF) (Van Veen et al., 1997). Beamformers can be used on the epileptic spikes (Bouet et al., 2012), but also on the continuous traces in combination with kurtosis mapping to identify the sources associated to IED and to reduce the amount of data to inspect (Hall et al., 2018). This latter procedure works by estimating the source time series for each position, called ‘virtual electrode’, in the source space grid and then computing the kurtosis value for each of these time series (Hall et al., 2018; Li et al., 2021; Wilenius et al., 2020). This method has been shown to be reliable and comparable to equivalent current dipole (ECD) techniques and validated by surgical outcomes (Hall et al., 2018; Wilenius et al.,

2020). The possibility to also detect deep epileptic sources was shown in two patients (Hillebrand et al., 2016).

A supposed advantage of ICA over the beamformer technique is a potential reduction of the cross-talk problem between sources (or ‘source leakage’), thanks to its sparsity. In fact, cross-talk manifests itself as a spurious connectivity between time series in the sources domain, due to the fact that “signals reconstructed at spatially separate brain locations are not necessarily independent” (Brookes et al., 2012) because of the smoothing introduced by the inverse problem and its ill posed nature. This is particularly important when studying connectivity, because even working at the source level, ‘source leakage’ may produce instantaneous artificial connections. Thus, connectivity measures that exclude the ‘zero-lag’ interaction have been suggested (reviewed in He et al., 2019). Conversely, the beamformer technique has the advantage of an intrinsic localization of the reconstructed sources, without requiring a further localization step.

In the present study, we exploited both simulated data and simultaneously acquired MEG and SEEG signals to compare ICA and LCMV-BF approach for characterizing the interictal epileptic dynamics. The aim of our study was to understand if ICA and LCMV-BF could be valuable approaches in identifying spiking sources and their dynamic network relations. With the simulation study, we stressed advantages and possible pitfalls of both the methods in a controlled framework. On spontaneous MEG data from eight epileptic patients, we further tested and compare the two methods performance evaluated with simultaneously recorded SEEG data (Badier et al., 2017).

2. Materials and methods

In this section, the datasets of simulated and real data are introduced. Then, the methods under analysis, are applied to both simulated and real data to point out their theoretical bases and assumptions. Finally, the procedure adopted to evaluate the interictal source separation and localization methods on simulated and the real data is described in details.

2.1. Simulated and real data description

2.1.1. Simulated data

Two simulation studies were carried out: SIM1 to explore the influence of the temporal and spatial correlation between two sources, and SIM2 to assess the possibility of retrieving the dynamic of a 3-source network configuration.

To obtain realistic MEG simulated data, we started from real imaging and MEG sensor locations from an epileptic patient with bilateral SEEG implantation and simultaneous MEG recordings. To model the head volume conductor, a boundary element method (BEM) model was obtained using OpenMEEG software in Brainstorm toolbox (Tadel et al., 2011). The BEM was computed from the cortex surface mesh with 15,005 vertices. The model was composed of three layers modeling the scalp and at each mesh vertex a dipole was modeled with unconstrained orientation. The obtained lead field was then used to project the sources, simulated as described below, to the 248 MEG sensors space.

To simulate the background activity (S_{BKG}), several intracerebral signals (monopolar SEEG channels) with no epileptic activity were selected from the patient and segmented in 5-second sections. The coefficients of an autoregressive (AR) model were estimated for each section (MATLAB LPC function) and averaged over the pieces of the same channel to have an estimate of the background activity. This procedure was previously implemented in (Roehri et al., 2017) to obtain realistic background brain noise. The Akaike information criterion (AIC) was employed to select the model order p .

The sources representing the background activity were uniformly distributed within the brain using 400 source positions composing the S_{BKG} . To simulate the interictal activity (S_{int}), an in-house MATLAB code was used which simulates time series with spikes waveform as a superposition of gamma distribution (Grova et al., 2006). By setting specific

parameters, such as probability of co-occurrence, time delay and jitter on the delay, it was possible to control the timing of the spikes and to simulate different levels of connectivity among the source activities. Time series representing S_{int} were associated to selected cortical patches.

Simulated signals X_{sim} are finally obtained as

$$X_{sim} = LF_{int} * S_{int} + \vartheta LF_{BKG} * S_{BKG} \quad (1)$$

where LF_{int} and LF_{BKG} are the leadfields associated to the selected active interictal sources and the background sources respectively and ϑ is a coefficient to tune the SNR at the sensors level. The leadfield of the sources was modeled by summing up the gain of the vertices within a cortical patch after constraining the source orientation to be normal to the cortex.

The SNR was estimated as the ratio between the variance of the interictal activity and the variance of the background activity averaged across sensors as in (2).

$$SNR = 10 \log_{10} \left(\frac{Var_{int}}{Var_{BKG}} \right) \quad (2)$$

For the simulation case SIM1, two sources were simulated. To modulate the temporal correlation, 13 different configurations of parameters were selected resulting in a temporal correlation (computed 'a posteriori') among the 2 sources spanning from 0.95 to 0.26. Since our interest was also on the effect of the spatial correlation between the two sources, after selecting the fixed patch S1 in the left frontal lobe, the second one was selected among the 400 patches of the uniform parcellation of the cortex performed in Brainstorm. The selection criteria were a decreasing mean spatial canonical correlation of its leadfield with the one of S1, and increasing distance, computed as Euclidean distance between their centroids. Repeating the procedure, eleven spatial configurations with two sources were obtained (S1 - Si, with i from 2 to 12) with a mean canonical correlation value in the range [0.99, 0.50] and distances ranging from 20 mm to 115 mm (Supplementary Fig. S1 displays the S1-S12 positions).

In SIM1, since our interest is on the effect of the correlation among the sources, a fixed SNR of 0 dB was used.

Three sources were simulated in SIM2, with a simpler temporal pattern of spike co-occurrences. Assuming that S1 is the first spiking source, spikes in the second source (S2) can occur with 0.7 probability after a spike occurrence in S1, with a 10 ms delay. In the third source (S3) the probability of occurrence of a spike after the occurrence in S1 was set to 0.5 and the delay was set to 30 ms. The three patches were selected in the frontal lobe, one in the left mesial position (S1) and two in the right hemisphere, one mesial (S2) and one in a distal position (S3). Spatially, S1 and S2 were selected to be the same in SIM1, and the final configuration used in SIM2 was inspired by an actual case. For the MEG signal in SIM2, the SNR was simulated at 5, 3, 1, 0, -1, -3 and -5 dB using the same background matrix.

Fig. 1 shows the simulation schema implemented in this work to obtain MEG simulated signals. In both cases, 5 min of data were simulated with a sampling rate equal to 2035 Hz, equivalent to the rate of the MEG recording system. Finally, simulated MEG signals were filtered between 1 and 45 Hz using a zero-phase FIR filter.

2.1.2. MEG and SEEG simultaneous recordings

Simultaneous MEG and SEEG recordings of 8 patients with drug-resistant epilepsies who underwent pre-surgical evaluation were included in this study (Table 1). Details of the recording procedure are provided in Badier et al., 2017. The ethical approval was obtained at the Comité de Protection des Personnes Sud Méditerranée I under ID RCB : 2012-A00644-39. For each patient, at least 10 min of simultaneous SEEG and MEG recording were obtained at rest either at the beginning or after a task session.

For all the patients, MEG Signals were acquired on a 4D Neuroimaging™ 3600 whole head system at a sampling rate of 2034.51 Hz with a total of 248 magnetometers. The simultaneous SEEG-MEG recording was carried out at the end of the long-term video-SEEG

monitoring period. SEEG and MEG were offline temporally aligned by resampling the SEEG from 2500 Hz to 2034.51 Hz (Badier et al., 2017).

For each patient, CT-scan/MRI data fusion was performed in order to find the anatomical position of each SEEG contact along the electrode trajectory. For this purpose, the in-house software GARDEL (a Graphical User Interface for Automatic Registration and Depth Electrodes Localization) was employed. This Matlab-based tool which allows the co-registration of MRI to the CT-scan, and the automatic segmentation and localization of contacts of depth electrodes by image processing (Medina Villalon et al., 2018). Only SEEG contacts localized in the gray matter were further considered and the signals were formatted in a bipolar configuration keeping only non-contiguous bipolar channels.

2.2. Interictal source separation and localization methods

2.2.1. Independent component analysis and dipole localization

Independent component analysis (ICA) is an approach for blind source separation widely used in MEG and EEG data analysis to separate the multivariate signal into additive and maximally statistically independent components (Comon, 1994). If the $N \times T$ matrix X represent the multivariate signals of length T samples recorded at the N sensors, ICA decomposes the signals in $M \leq N$ components having a corresponding time series in the $M \times T$ matrix S and a spatial representation given by the weight matrix W using the observation model given in Eq. (3)

$$X = WS. \quad (3)$$

Here, the Infomax algorithm (Bell and Sejnowski, 1995) was chosen to unmix the MEG data and identify components associated to interictal spiking activities with no priors about their occurrences (Kobayashi et al., 1999). Specifically, this algorithm searches for independent components with a distribution showing positive kurtosis (super Gaussian distribution) and identifies a weight matrix W which maximizes the entropy of the set of independent sources. Each independent component carries both a spatial and a temporal information. The spatial information can be used to localize the component (Barborica et al., 2021; Kobayashi et al., 2002, 1999; Pizzo et al., 2019).

In this work, for the MEG forward calculation, we used a single shell spherical head model as implemented in FieldTrip (Oostenveld et al., 2011), building a regular grid within the brain volume (10 mm of spatial resolution). At each point of the 3-dimensional grid, a triplet of orthogonal dipole was positioned. A linear regression was performed to fit the dipole model into the selected IC map and retained the resulting best goodness of fit (GOF) (Pizzo et al., 2019). The same head model was also used to reconstruct the sources with the beamformer techniques as explained in the next section, to provide a basis for the source localization comparison.

2.2.2. LCMV beamformer and kurtosis mapping

The linearly constrained minimum-variance beamformer (LCMV-BF) is a source localization and reconstruction technique, proposed by (Van Veen et al., 1997), and implemented in many toolboxes (Jaiswal et al., 2020). It is based on the application of a spatial filter that associates the magnetic field measured by the MEG sensors outside the brain to the neural activities within the brain. It exploits the covariance of the recorded signals and does not require prior assumption on the number of active sources. The weights of the spatial filter that transfer information from the sensor to the brain sources are computed at each location at the positions of interest in the brain. The same equation presented in (1) can be used to describe the model, but in this case the matrix S contains the sources at any location of interest in the brain, and the number of sources M can be much greater than the number of sensors N , while W represents the leadfield. The latter is used in the beamformer calculation, to obtain a $N \times 3$ spatial filter at each source location that allows estimating the source time-courses from sensor data (Jaiswal et al., 2020; Sekihara et al., 2002; Van Veen et al., 1997). By applying the obtained spatial filters to the MEG data, the output of the

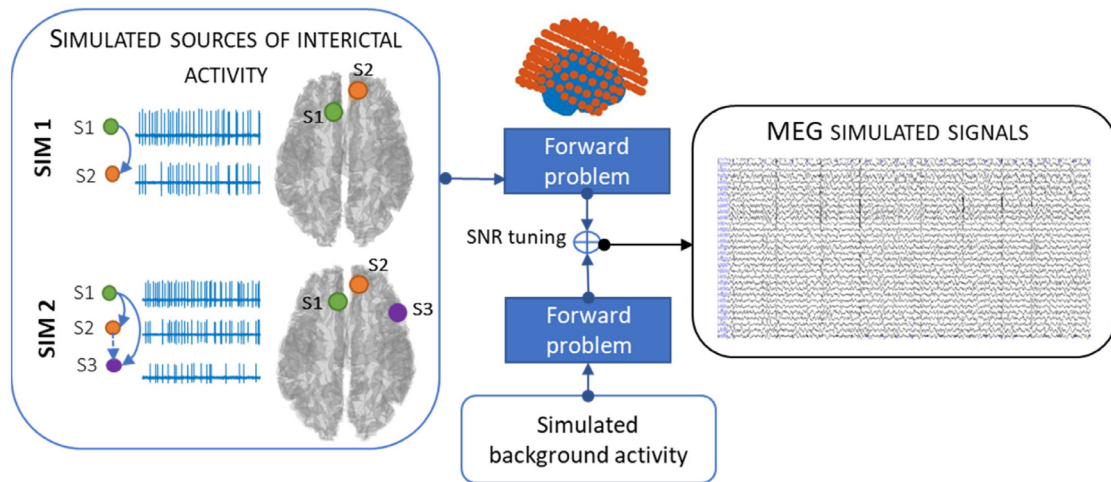


Fig. 1. Summary of the simulation procedure. In both SIM1 and SIM2, and for each selected source position, a time series is simulated with interictal activity, and a propagation pattern is imposed among them in terms of events co-occurrences and delays. The forward model is then solved to compute the activity at the MEG sensors. The background activity was simulated in a similar way and added to the simulation at a given SNR.

Table 1
Patients' information.

ID	AGE AT SEEG	GENDER	IMPLANT SIDE; EPILEPSY TYPE	AGE AT EPILEPSY ONSET	EPILEPSY DURATION	ENGEL SCORE
PAT 1	19	M	Bilateral; Frontal	2	17	Ia
PAT 2	41	F	Left; Temporal	34	12	IVb
PAT 3	29	F	Bilateral; Temporo-occipital	19	10	NA
PAT 4	33	M	Right; Insulo-parieto-premotor	1.5	31	NA
PAT 5	22	M	Bilateral; Temporal	2	19	III
PAT 6	45	F	Bilateral; Parietal mesial and temporo-basal	11	34	III
PAT 7	33	M	Bilateral; Temporal	11	22	NA
PAT 8	57	M	Left; Temporal and Parietal	39	18	IA

beamformer is thus a time series for each target location representing the activity of that source. To identify the source of interictal activity, associated with the presence of interictal spikes, we performed a Kurtosis mapping (Kirsch et al., 2006). This procedure consists in computing the Kurtosis for each obtained virtual electrode time series resulting in a volumetric map. The identification of candidate interictal epileptic sources is based on the detection of local maxima in the volumetric map, as high kurtosis has been used as a marker for spiking activity (Hall et al., 2018; Li et al., 2021).

2.3. Connectivity analysis

We selected the cross-correlation index as it is a simple linear connectivity method, widely used in the analysis of SEEG and MEG data in presence of ictal and interictal events (Hassan et al., 2017; Jmail et al., 2016). Specifically, the cross-correlation coefficient R^2 quantifies the correlation between two signals $x(t)$ and $y(t)$ in function of a time delay or lag l between them. It is computed as in (4)

$$R^2 = \max_l \frac{\text{cov}^2(x(t), y(t+l))}{(\sigma_{x(t)}\sigma_{y(t+l)})^2} \quad (4)$$

where σ is the standard deviation of the data, cov indicates the covariance. We applied the cross-correlation on continuous data with a 1-second sliding window without overlap for a series of lags (± 100 ms), and kept the lag corresponding to maximum correlation, as implemented in the AnyWave software (Colombet et al., 2015).

2.4. Simulated data analysis

ICA infomax, LCMV-BF and dipole fitting were performed using Fieldtrip-based scripts (Oostenveld et al., 2011) with the single-shell

head model type as previously stated. This was decided to simulate a real situation in which the head model used is the single shell spherical one and to avoid a possible bias due to the use of the same model to produce and analyze simulations ('inverse crime', Colton and Kress, 1992; Lamus et al., 2012). The analysis schema is reported in Fig. 2, where the analysis applied to simulated data is highlighted in italic.

ICA was applied with a dimensionality reduction using principal component analysis (PCA) to extract 50 and 100 components. ICs presenting the simulated spiking activity were visually selected. These were then localized by means of single dipole fitting with an interval of confidence method (IoC) (Pizzo et al., 2019).

LCMV-BF spatial filter was applied to the data scanning the 3D grid built in the brain volume with the order of 3000 positions (10 mm resolution). For each point of the grid within the brain volume, a time series was obtained representing the reconstructed activity of each dipole. For each time series the kurtosis value was computed and for comparison to the spiking ICs, the beamformer virtual electrodes associated with the highest local maxima of kurtosis values were retained. After visually checking the results, the highest two (SIM1) or three (SIM2) virtual electrodes were further considered.

2.4.1. Source identification

The Pearson's correlation coefficient R was computed between the reconstructed interictal activity and the source simulated activity considering the concatenated spike events. Results of the correlation were used to derive an index for the quality of the reconstruction ($QofR$) in each condition (varying temporal and spatial correlation or varying SNR).

Specifically, in SIM1, for each of the 143 realizations (corresponding to 11 spatial configurations and 13 temporal correlation levels) only two independent components, both for ICA 50 and ICA 100, and two virtual

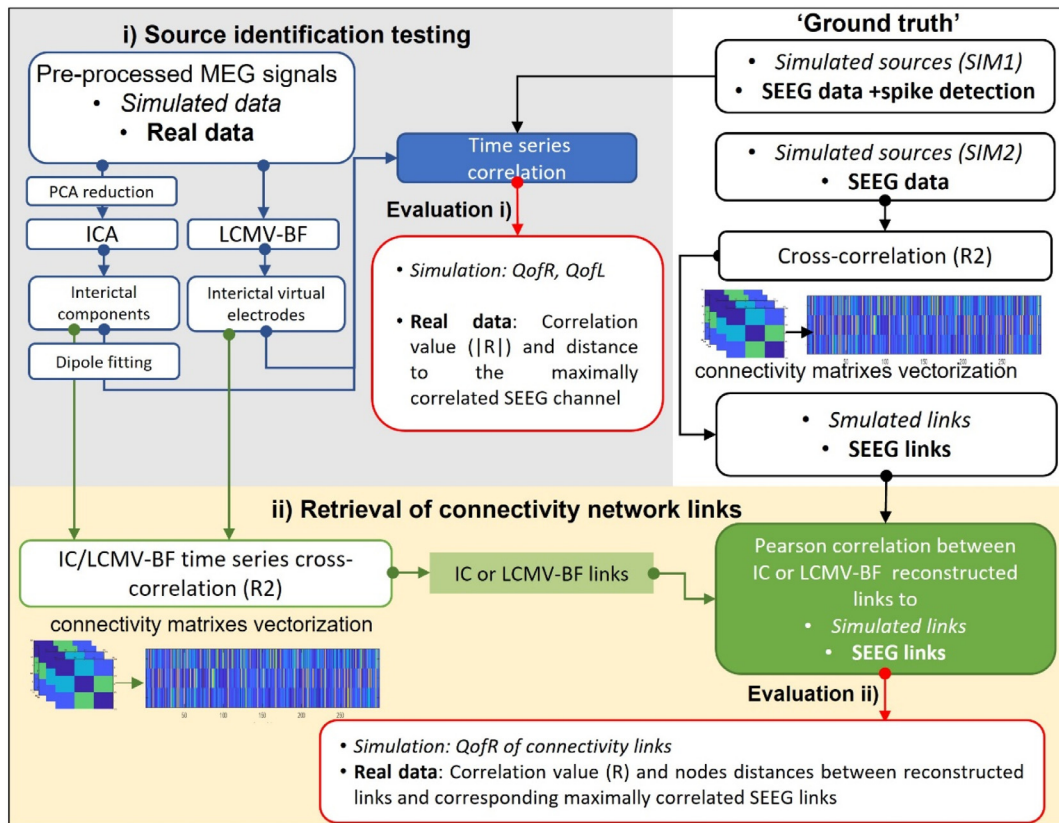


Fig. 2. Overview of the pipeline for data analysis. The evaluation scheme is similar for both simulated and real data, with needed differences that are highlighted using *italic* for simulated data and **bold** for real data. The procedure comprises two main evaluation steps: i) the analysis of the time series reconstruction and source localization (blue edges and arrows in the gray box), and ii) the evaluation of the correspondences between SEEG (or simulated sources) and MEG-derived connectivity (green edges and arrows on yellow box). For the simulations, the ‘ground truth’ refers to the different spatial and temporal configurations of SIM1, and the three-source simulation with connectivity pattern of SIM2. The evaluation is based on the two indices for the quality of the time series reconstruction (*QofR*) and for the quality of the sources localization (*QofL*). For the real data, SEEG time series and their connectivity patterns are considered as ‘ground truth’.

electrodes (highest local maxima of the kurtosis map) were expected to capture the simulated interictal sources. In SIM 2 we expected to find three sources for each method and condition. Then the selected reconstructed sources were matched with the simulated one based on their correlation value.

We obtain a 2×2 (SIM2) or 3×3 (SIM2) correlation matrix (i.e., for each spatial/temporal combination and each SNR) where on the main diagonal we put the absolute correlation $|R|$ of the matched time series and on the off-diagonal element the un-matched time series. To summarize the results, the correlation matrix obtained for each realization was compared to the ideal, one having $|R| = 1$ on the main diagonal and the $|R|$ computed between the two simulated sources on the off-diagonal. The comparison was then quantified as $QofR = 1 - d$, where d is the Euclidean distance between the two correlation matrices. By construction, the obtained measure has an upper limit equal to 1 indicating perfect reconstruction.

Localization errors were estimated by computing the Euclidean distance of the estimated position from the center of the corresponding simulated sources on the grid. To summarize the localization performances, similarly to the activity reconstruction, a ‘quality of localization’ measure was derived in the same way by considering as an ideal result a matrix having a main diagonal set to 0 (perfect localization) and on the off-diagonal the distance between the simulated sources. By computing the Euclidean distance (d) between the localization results and the ideal set, the summarizing measure was defined as $QofL = 1 - d$. Again, an upper limit equal to 1 indicated perfect localization.

A further assessment was made to estimate the cross-talk effect. The correlation among the reconstructed activities (ICs and LCMV-BFs sep-

arately) was performed considering windows in which S1 presented a spike but no co-occurring spikes were present in S2, meaning that a high correlation values between the two reconstructed sources in that specific windows indicate the presence of ‘phantom’ events on the component (or virtual electrode) associated to S2. We used the resulting $|R|$ value as an estimation of cross-talk. Only the cases where all the methods detected at least two sources were considered, corresponding to the cases with a delay between co-occurring events.

2.4.2. Retrieval of connectivity network links

The cross-correlation (R^2) was computed between the time series of the simulated sources (SIM2) and between the selected ICs and virtual electrodes separately, resulting in a connectivity matrix for each second (because of 1 s windows calculation) of simulated data for the three datasets (simulated sources or ‘gold standard’; selected ICs; selected LCMV-BF time series). To compare the reconstructed and simulated connectivity evolution in time, the connectivity matrixes were vectorized at each time point considering the upper triangle as it is symmetric, and the temporal evolution of each reconstructed link was compared to the one of the simulated connections. To quantify the degree of agreement between the two dynamics, a partial correlation was computed: the correlation between the reconstructed link and the simulated ones is measured, controlling for the other two reconstructed links in order to remove their influence. Then the matched and unmatched dynamics are compared between reconstruction methods as a function of the SNR level (SIM2). Similar to the time series correlation analysis, a *QofR* measure was obtained by comparing the correlation matrix acquired from the link correlation analysis to the identity matrix in this instance, since

we expect null-values for off-diagonal elements when employing partial correlation.

2.5. Real data analysis

Fig. 2 also shows the analysis scheme applied to real data. SEEG data were band-pass filtered in the 1–45 Hz frequency band with a zero-phase FIR filter. Spike detection (Delphos v1.0.1, (Roehri et al., 2016)) was applied to the SEEG channels presenting visible spikes and then manually checked and confirmed. The channel with the largest number of spikes was further considered as the reference channel in the subsequent analysis. MEG signals were filtered between 1 and 45 Hz with a zero-phase FIR filter before the application of independent component analysis (ICA) and LCMV beamformer (LCMV-BF). After bad channels and large artifacts removal, Infomax algorithm was applied to the filtered MEG signals with PCA dimensionality reduction to 100 components, as simulations show slightly better performance with respect to the extraction of only 50 components.

For further analysis, ICs presenting interictal activity were visually selected and confirmed by an expert epileptologist (F. Bonini). These were then localized by means of single dipole fitting with interval of confidence method (IoC). For the IoC method, a linear regression was computed to compare each ICA map to the model composed by those triplets and retained the resulting maximum goodness of fit (GOF). The best position is retained accordingly, and only the ICs having a GOF >75% were further analyzed (Pizzo et al., 2019).

LCMV beamformer spatial filter (Van Veen et al. 1997), was applied to the filtered MEG data scanning the 3D grid built in the brain volume. For further analysis and for comparison to the spiking ICs, the virtual electrodes identified as local maxima of the volumetric kurtosis map, were visually checked, and confirmed by the expert to ensure that the high value of kurtosis was due to the presence of interictal activity and not to artifacts.

2.5.1. Source identification

Invasive (SEEG) and non-invasive (ICA 100 and LCMV-BF) data were segmented in 1 second epochs around each spike according to the SEEG detection timings, and the segments were concatenated. A first analysis, to understand the activity captured, was a linear correlation analysis between each SEEG bipolar channel and the reconstructed MEG-based time series.

Therefore, the measures of interest were:

- Pearson's correlation ($|R|$) between each MEG-based reconstructed interictal source and SEEG signals, only correlations with an associated p-value <0.05 were considered.
- Distance (D) between the estimated position of the source and the mostly correlated SEEG channel.

We assume that the mostly correlated SEEG channel represents the source that is being localized (Fahimi Hnazaee et al., 2020). Anyway, this is not guaranteed and may depend on the SEEG implantation scheme (Velmurugan et al., 2022). For each patient, a different number of independent components and virtual electrodes are associated to interictal activity and a one-to-one correspondence among methods is not possible. Thus, for each independent component and LCMV-BF virtual electrode, only the maximum correlation value and the corresponding distance from the correlated SEEG bipolar channel was further considered.

2.5.2. Retrieval of connectivity network links

To assess the possibility of retrieving network organization from MEG exploiting either the sparsity of the ICA or the beamforming technique, we correlated the MEG based network (MEG-net) to the SEEG network (SEEG-net). The idea was to observe the dynamic evolution of each network link reconstructed from MEG and to identify the corresponding links of the SEEG-net thanks to the correlation between link

time-courses. Of note, for real data we used classical correlation instead of partial correlation because the number of variables to control for were not fixed.

As for the correlation between time-series and for a representative evaluation, the maximum positive and significant ($p < 0.05$) correlation of each MEG-net/SEEG-net link pair was identified. For each considered link, we computed the Distance 1 (mm) as the distance between the closest MEG-net/SEEG-net node of the link and Distance 2 (mm) as the distance between the remaining MEG-net/SEEG-net node. The mean of the two distances was then used for the comparison of localization methods.

As for the time series correlation analysis, a different number of invasive and non-invasive links characterizes each patient. To simplify the comparison, only the maximum correlation for each MEG-net link was considered and the associated distances from the correlated SEEG-net link were computed.

2.5.3. Estimation of signal-to-noise ratio

To better interpret the results, we estimated the signal-to-noise ratio (SNR) of MEG signals in each patient considering as signal of interest the interictal activity and as noise the background activity. We used the spike timings obtained from the SEEG and computed the signal variance ($\text{Var}_{\text{Spike}}$) in a 200-ms window centered on the peak of each spike and the noise variance (Var_{BKG}) in a 200-ms window composed of 100 ms pre- and 100 ms post-spike signal (Pizzo et al., 2019). The resulting SNR, computed according to (4), was averaged across events at each MEG sensor position. The same approach was used to estimate the SNR of the ICs and of the selected LCMV virtual electrodes.

2.6. Statistical analysis

To assess statistical differences among methods in the SIM1 study, QofL and QofR indexes were tested for normality with the Kolmogorov-Smirnov test. Consequently, the non-parametric Friedman's test was employed followed by a multiple comparison analysis, corrected according to the Bonferroni's approach considering the three groups. The same analysis was applied also to test the cross-talk effect.

A linear mixed effects (LME) analysis to explain possible differences among the methods was instead applied to real data, considering separately the correlation (R) and the distances (D) in both the analysis paths: i) source identification, and ii) retrieval of connectivity network links. As a fixed effect we use the 'source type' (i.e., ICA100 or LCMV-BF) and as random effect the patients. This was necessary because each patient had a different number of identified sources according to the method, thus it was necessary to account for the inter- and intra-patient variability.

Furthermore, to infer significances across patients, we applied the local false discovery rate (LFDR) (Benjamini and Heller, 2007) on the correlation values to identify a threshold of significance corresponding to an alpha level of 0.05 and fitting a beta distribution (model of H0) in both analysis paths i) and ii). Consequently, we counted the number of correspondences above the threshold and their associated distances.

3. Results

3.1. SIM1: source identification

Fig. 3 shows results obtained from SIM1. In terms of QofR (Fig. 3a), ICA showed low values with both 50 and 100 extracted components for the high temporal correlation conditions. For the case of complete correlation, only one spiking component could be found preventing the correct source separation, but the introduction of a small delay between the occurring events in the two sources resulted in improved ICA performance. Decreasing temporal correlation, the obtained results were comparable to the ones obtained by the LCMV-BF. Considering the spatial configurations, ICA seemed stable across different relative positions

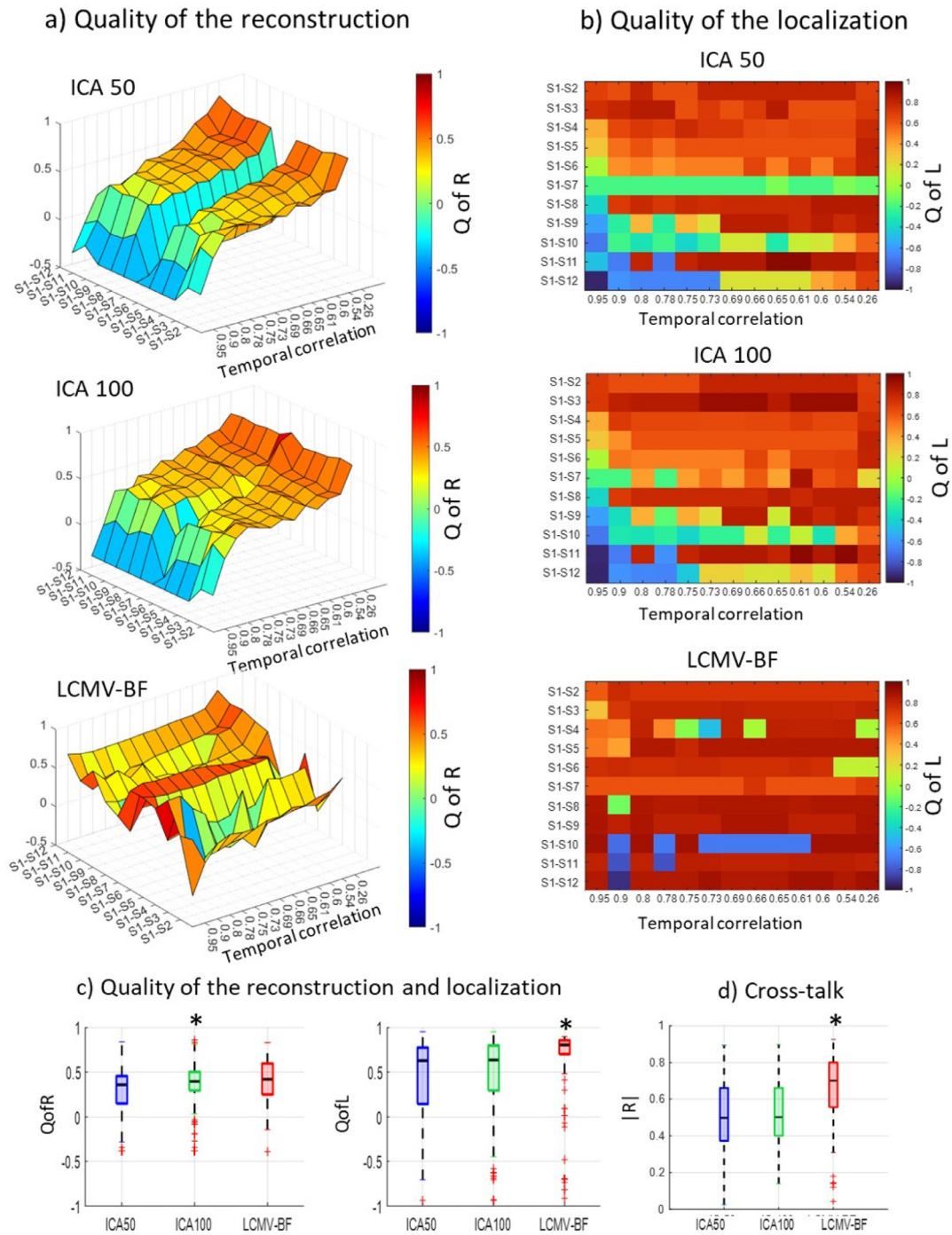


Fig. 3. Time series correlation results. a) The Quality of the reconstructed activity is shown in function of the spatial and temporal correlation for the three methods. Z-axis scale is the same as in the colormap. b) for each method the Quality of the localization is displayed in function of the spatial and temporal correlation. c) box-plot comparing the two measures considering all the 143 conditions at once, * indicate the statistically higher QofR and QofL. d) Quantification of the crosstalk effect through correlation values computed in correspondence of non-occurring events. The beamformer method showed a slightly but significantly higher crosstalk effect (*) with respect to both the ICA types, that were not different between themselves.

except for patch S7 where the source positioned in a deep portion of the cortical mesh was not detected by ICA with 50 components, while the situation improved with 100 ICs.

LCMV-BF results were less affected by the temporal correlation than ICA. LCMV-BF showed a stable performance against temporal correlation levels, but its behavior in function of the position of the two sources was difficult to predict. Comparing the overall results, ICA100 yielded higher *QofR* values than the other two methods (ICA100>ICA50 with p-

value <10⁻⁵; ICA100>LCMV-BF with p-value = 0.005), as determined by Bonferroni-corrected post-hoc analysis after the non-parametric statistical Friedman test (Fig. 3. c).

Results of the quality of the localization using dipole fitting for ICA and the identification of the local maxima position in the Kurtosis map are shown in Fig. 3b. Using the same grid for the two methods, better results were obtained for the LCMV-BF. This was particularly evident when the two sources were highly correlated in time but distant.

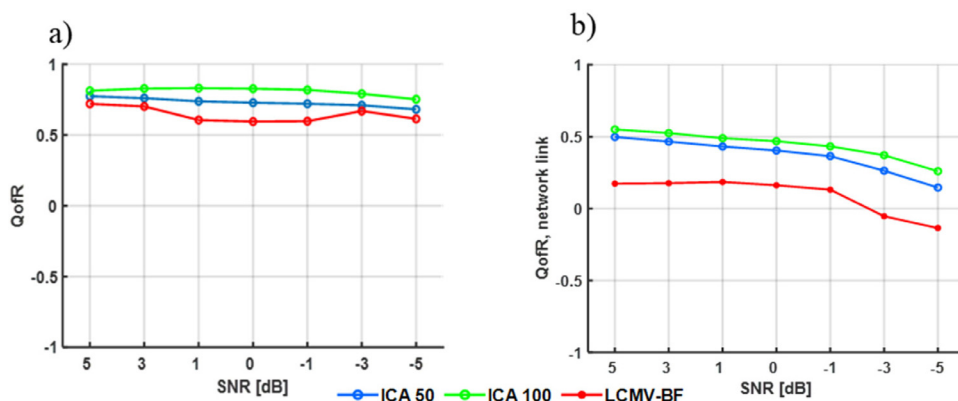


Fig. 4. a) QofR, in function of the decreasing SNR level, associated to the time series reconstruction, b) QofR, in function of the decreasing SNR level, associated to the correspondences between the network links of the MEGnet and the SIMnet.

Table 2

Number (#) of identified and selected independent components and virtual electrodes. Numbers within brackets indicate the further analyzed ICs (with GOF>75%). The estimated MEG SNR (in dB) averaged across channels and maximum values are shown.

ID	number of selected ICs/LCMV-BF		MEG SNR (dB)	
	# ICA-100	# LCMV-BF	Mean	Max (averaged on events)
PAT1	5 (4)	5	1.55	4.77
PAT2	8	7	2.32	5.13
PAT3	3	6	0.47	1.39
PAT4	4 (3)	8	0.13	1.04
PAT5	15 (10)	10	-0.32	0.86
PAT6	6 (2)	10	-0.08	0.65
PAT7	5 (4)	8	-0.17	0.58
PAT8	4 (2)	8	0.04	1.17
tot	50 (36)	62	MEAN (SD)	0.49 (0.94)
				1.95 (1.87)

This is explainable since this combination of conditions lead to components with a non-dipolar topography that cannot be resolved with one dipole only. Perfect correlation between generators is unlikely in real cases, but it pointed out with an extreme example a main limitation of ICA. Concerning LCMV-BF, results were stable except for few incorrect performances, leading to a statistically higher *QofL* values with respect to both the groups of extracted components (i.e., LCMV-BF > ICA50 with p -value < 10⁻⁵; LCMV-BF > ICA100 with p -value < 10⁻³) according to Bonferroni corrected post-hoc analysis following the non-parametric statistical Friedman test (Fig. 3c). Results are shown in Fig. 3d, where slightly but significantly higher cross-talk effect can be observed for the LCMV-BF (Friedman test < 0.01; post-hoc test with Bonferroni's correction: LCMV-BF > ICA100 p = 0.002; LCMV-BF > ICA50 p < 10⁻⁴).

3.2. SIM2: retrieval of connectivity network links

At each SNR level of SIM2 three ICs, both for ICA 50 and ICA 100, and three virtual electrodes (highest local maxima of the kurtosis map) were further analyzed. These were assumed to capture the simulated connectivity pattern. In general, the ICA-based network showed a better performance with respect to the LCMV-BF, as can be appreciated in Fig. 4 where *QofR* results are plotted in function of the SNR, both for the simple time-series correlation (Fig. 4a) and for the reconstruction of the connectivity links (Fig. 4b). Since partial correlation was used in this case, the ideal matrix was set to be simply the identity matrix. Of note, for the localization performance, the position of the sources - inspired by a real patient epileptogenic network - were easily identified by all the methods, with a more stable performance for the LCMV-BF.

3.3. Real data

In this section, results obtained on the real dataset are described. Since the simulation analysis showed a better performance of the

ICA100 with respect to ICA50, only results related to the first approach are discussed here in comparison to the LCMV-BF.

In Table 2, the details of the identified interictal sources (selected ICs and LCMV-BF) and of the SNR values estimated at the MEG sensors for each patient are reported. We verified that both methods were able to detect interictal sources from MEG data without the need for averaging or detect spikes prior to their application (supplementary Table S1). An illustrative example regarding PAT1 is shown in the supplementary Fig. S2 where a time segment of 10 s is displayed for MEG, SEEG and each source separation method.

3.3.1. Source identification: SEEG informed signal time-series correlation

An illustrative example of the correlation analysis is shown in Fig. 5, where the correlation matrices (sources vs SEEG channels), the three-dimensional representation of the highest correlation value between ICs/LCMV-BF virtual electrodes and the SEEG time series, as well as the averaged spike waveform are shown for a representative patient (PAT3). The polarity of the SEEG and the source signal may be the opposite, but still they gave high $|R|$ values.

Both methods identified a good match (high $|R|$ and low Distance) with the SEEG channel TB6-TB7 in the right temporal lobe and the source localized in its proximity (IC4 and bf519 respectively). Based on the same criteria to select good matches, a direct comparison is reported in the supplementary Table S2, where a concordance of methods (i.e., a source correlated and close to the same SEEG channel) is found in five patients.

Fig. 6a illustrates the large variability across patients. The obtained statistical threshold on correlation values across methods and patients was equal to 0.34. It resulted that in six out of eight cases, both methods showed at least one significant value above the threshold. PAT6 and PAT7 presented low $|R|$ values with only one significance in LCMV-BF and ICA respectively. Specifically, the 50% of the ICs selected were also correlated above the statistical threshold, while only the 34% of the

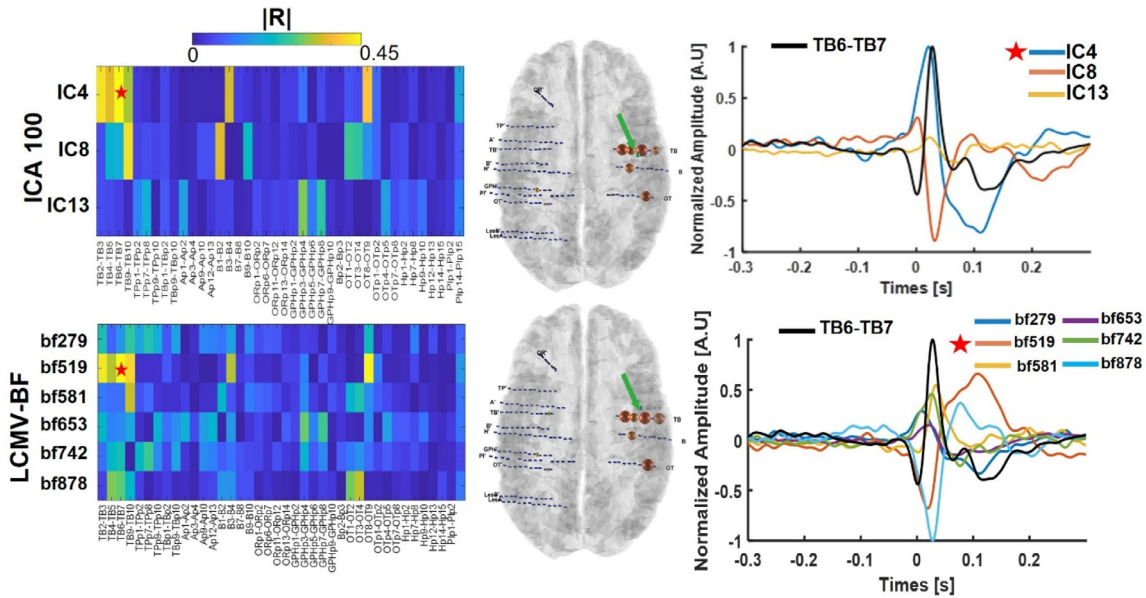


Fig. 5. Example of the time series correlation results in a subject (PAT3) showing very similar performances for ICA-100 and LCMV-BF in terms of correlation values ($|R|$) and distance between the localized source and the mostly correlated SEEG channel. On the left, the correlation matrix among reconstructed activities (sources) and all the bipolar SEEG channels is displayed (red star indicates the highest $|R|$ value). In the middle, the 3-dimensional representation of the best match (source-SEEG) is shown in the middle and the correspondence to the red star on the matrix is indicated by the green arrow. On the right, the averaged spikes.

selected LCMV-BF sources were. For PAT1, PAT2, PAT3 and PAT4, ICA showed slightly better results than LCMV-BF in terms of correlation values and associated distances between the sources estimated position and the matched SEEG channels, as can be observed also in Table 3. Interestingly, these patients were the ones with the highest estimated SNR conditions. Moreover, in these patients (and PAT8), the two methods were concordant in identifying the interictal sources, that is, they both identified at least one source of epileptic spikes in proximity of the same SEEG channels with also a good correlation of their activity (Table S2).

PAT5 was a particular case. The patient had already undergone surgery for epilepsy treatment prior to SEEG (resection of the left temporal gyrus) with poor surgical outcomes and persistence of drug resistant seizure. No further abnormalities were present in the new MRI. The patient’s second SEEG still presented frequent superficial spikes (detectable on the scalp and on cortical activity) with apparently independent sources in the left hemisphere and large propagation networks which were reflected by evident interictal activity on MEG captured by several components. Probably because of high temporal correlation of the sources participating in the network, the first component reflected itself a network organization and resulted in being highly correlated to many bipolar SEEG channels (Supplementary Fig. S3). This could also explain the large interval of confidence in the dipole fitting procedure

including more than 17% of the grid points and a maximum GOF of 77%. In this patient, three out of ten ICs had significant $|R|$ values, while six out of ten sources were significantly correlated to SEEG channels for the beamformer method. On average, a better performance was given by the LCMV-BF.

Finally, PAT6, PAT7 and PAT8 showed comparable results for the three methods, with slightly better performances in terms of distance between the positions of the interictal sources and the matched SEEG channels for the LCMV-BF technique. In fact, probably due to a lower SNR, the topography of the selected components for PAT6 and PAT8 were not perfectly dipolar leading to a non-optimal localization and only 2 ICs with acceptable GOF (>0.75).

No significant difference was found for the absolute correlation $|R|$ (p -value = 0.078) and the distance from the mostly correlated SEEG contact D (p -value = 0.136) by fitting a linear mixed effect model on the data. ICA reached overall a higher correlation value associated with a lower average distance. Therefore, it may be interesting to investigate the two measures together, as in Fig. 6b where the correlation value between the reconstructed source (i.e., ICs or LCMV-BF sources) and the maximally correlated SEEG bipolar channel are displayed as a function of their distance. One can appreciate that the values of correlation above threshold (dashed line) are associated to lower distances and that, on

Table 3

Median and min-max range of the correlation and distances values for each patient and method. In bold the best performance for each patient. The number of reconstructed sources with correlation above the LFDR threshold is also shown with the maximum estimated SNR.

ID	ABS(R) VALUES		DISTANCE (mm)		# OF SIGNIFICANCE		MAX SNR (AVERAGED ACROSS EVENTS)	
	ICA 100 Median (min -MAX)	LCMV-BF Median (min -MAX)	ICA 100 Median (min -MAX)	LCMV-BF Median (min -MAX)	ICA 100 #	LCMV-BF #	ICA 100 dB	LCMV-BF dB
PAT1	0.474 (0.228–0.576)	0.356 (0.203–0.447)	28.0 (14.1–39.6)	43.7 (22.8–51.6)	3	3	5.49	3.40
PAT2	0.501 (0.174–0.564)	0.357 (0.241–0.509)	9.9 (5.7–57.7)	22.6 (9.2–40.0)	6	5	7.92	6.40
PAT3	0.454 (0.323–0.487)	0.321 (0.260–0.463)	24.3 (13.9–25.9)	42.4 (18.0–73.0)	2	3	2.23	2.43
PAT4	0.413 (0.168–0.557)	0.250 (0.174–0.519)	24.1 (6.9–44.9)	64.1 (12.9–4.4)	2	1	1.52	0.65
PAT5	0.276 (0.102–0.815)	0.364 (0.233–0.467)	38.6 (18.3–115.4)	31.5 (12.0–51.5)	3	6	1.78	1.85
PAT6	0.225 (0.141–0.310)	0.192 (0.101–0.363)	40.7 (33.1–48.3)	22.8 (13.5–99.7)	0	1	0.33	0.50
PAT7	0.274 (0.117–0.350)	0.231 (0.157–0.307)	36.2 (10.2–56.8)	21.7 (8.5–94.7)	1	0	0.60	0.31
PAT8	0.274 (0.115–0.433)	0.323 (0.145–0.391)	35.5 (5.4–55.5)	26.3 (13.1–48.4)	1	2	1.40	2.82

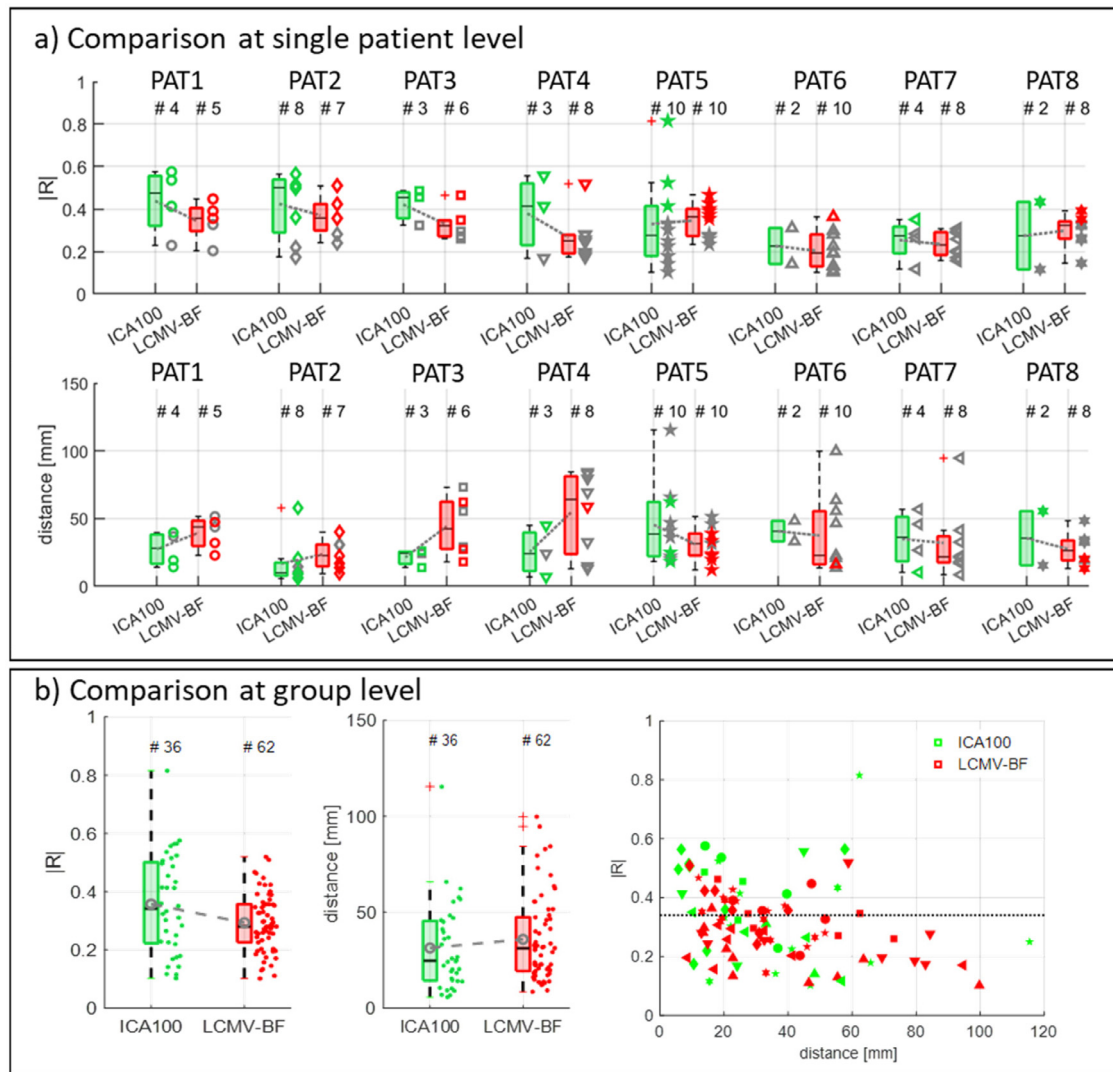


Fig. 6. Real data results on the signal time courses. a) boxplots comparing the correlation coefficient and the distance across methods for each patient (the number # of ICs and LCMV-BFs is reported above). Gray markers identify under threshold R values and the associated distances. b) shows boxplots for $|R|$ values and distances at group level and the scatterplot of correlation values between reconstructed sources and the mostly correlated SEEG channels ($|R|$) in function of their distance, different markers indicate different patients accordingly to panel a), the dashed line indicates the LFD threshold across all the $|R|$ values.

average, ICs reached a better trade-off between distance and correlation value.

3.3.2. Retrieval of connectivity network links: correlation of MEG-net and SEEG-net dynamics

For each link of the MEG-net, the mostly correlated SEEG-net link was identified, and compared against the obtained LFD threshold = 0.238. **Supplementary Fig. S4** shows an example of the temporal evolution of connectivity links for both the MEG network and the ones of the corresponding SEEG network for PAT1. It also displays results from three representative patients. For a direct comparison between the methods, the most concordant SEEG-net/MEG-net matches, among the two methods, are reported in **supplementary Table S3**.

Considering all the possible SEEG/MEG correspondences, we obtained the results shown in **Table 4** and **Fig. 7**.

From **Fig. 7a**, it is possible to notice that PAT6 had no significant correspondences, similarly, PAT8 only showed acceptable results with the LCMV-BF method. PAT1 and PAT2 were better characterized using ICA, even if in the latter case the median R values obtained with the two methods were equal, but with lower distances when using ICA. Patients PAT3 and PAT5 were characterized by similar results with the two

methods, but with opposite trends: higher R values for ICA and lower distances for LCMV-BF in PAT5, the opposite behavior in PAT3. Finally, PAT7 and PAT4 both showed only one correspondence above threshold with ICA, more than 10 with LCMV-BF but with large variability in the distances. Therefore, when considering the dynamics of the connectivity links, a clear correspondence between high R values and low mean distance was not observed as shown in the scatterplot (**Fig. 7b**), where the cloud of points is wider along the distance axis. Across all the patients, no significant differences were found between the two methods (**Fig. 7b**). It is also important to notice that the R values, obtained at the links level, were evidently lower than the ones obtained for the time series correlation analysis. This is easily explained by the fact that in the connectivity case we did not consider the information provided by the spike timings, but we analyzed the dynamic of the networks along the whole 10-minute recording.

4. Discussion

It has been proven, through a plethora of analysis methods, that MEG non-invasive recordings help the characterization of the epileptogenic network and, therefore, the presurgical evaluation (Grova et al., 2016;

Table 4

Median and min-max range of correlation values and sum of distances among outside/inside links for each patient and method.

ID	R values		Mean(D1, D2) [mm]		Number of significances	
	ICA 100	LCMV-BF	ICA 100	LCMV-BF	ICA 100	LCMV-BF
	Median (min -MAX)	Median (min -MAX)	Median (min -MAX)	Median (min -MAX)	#	#
PAT1	0.326 (0.222–0.423)	0.278 (0.163–0.428)	32.73 (12.71–45.78)	38.26 (22.30–51.40)	5	6
PAT2	0.228 (0.178–0.495)	0.229 (0.115–0.293)	31.66 (7.81–52.88)	44.19 (13.49–67.27)	11	8
PAT3	0.159 (0.152–0.282)	0.217 (0.157–0.333)	19.90 (13.89–47.82)	43.85 (27.22–50.81)	1	3
PAT4	0.196 (0.170–0.269)	0.221 (0.162–0.328)	31.79 (16.10–36.35)	54.94 (21.62–76.80)	1	12
PAT5	0.214 (0.133–0.401)	0.199 (0.119–0.286)	53.06 (19.13–94.36)	44.42 (17.25–107.36)	13	6
PAT6	0.138 -	0.141 (0.117–0.188)	43.70 -	51.32 (23.54–92.73)	0	0
PAT7	0.158 (0.138–0.290)	0.239 (0.139–0.320)	46.34 (15.10–66.29)	47.13 (25.51–84.38)	1	14
PAT8	0.152 -	0.167 (0.127–0.249)	39.53 -	39.40 (16.44–84.35)	0	2

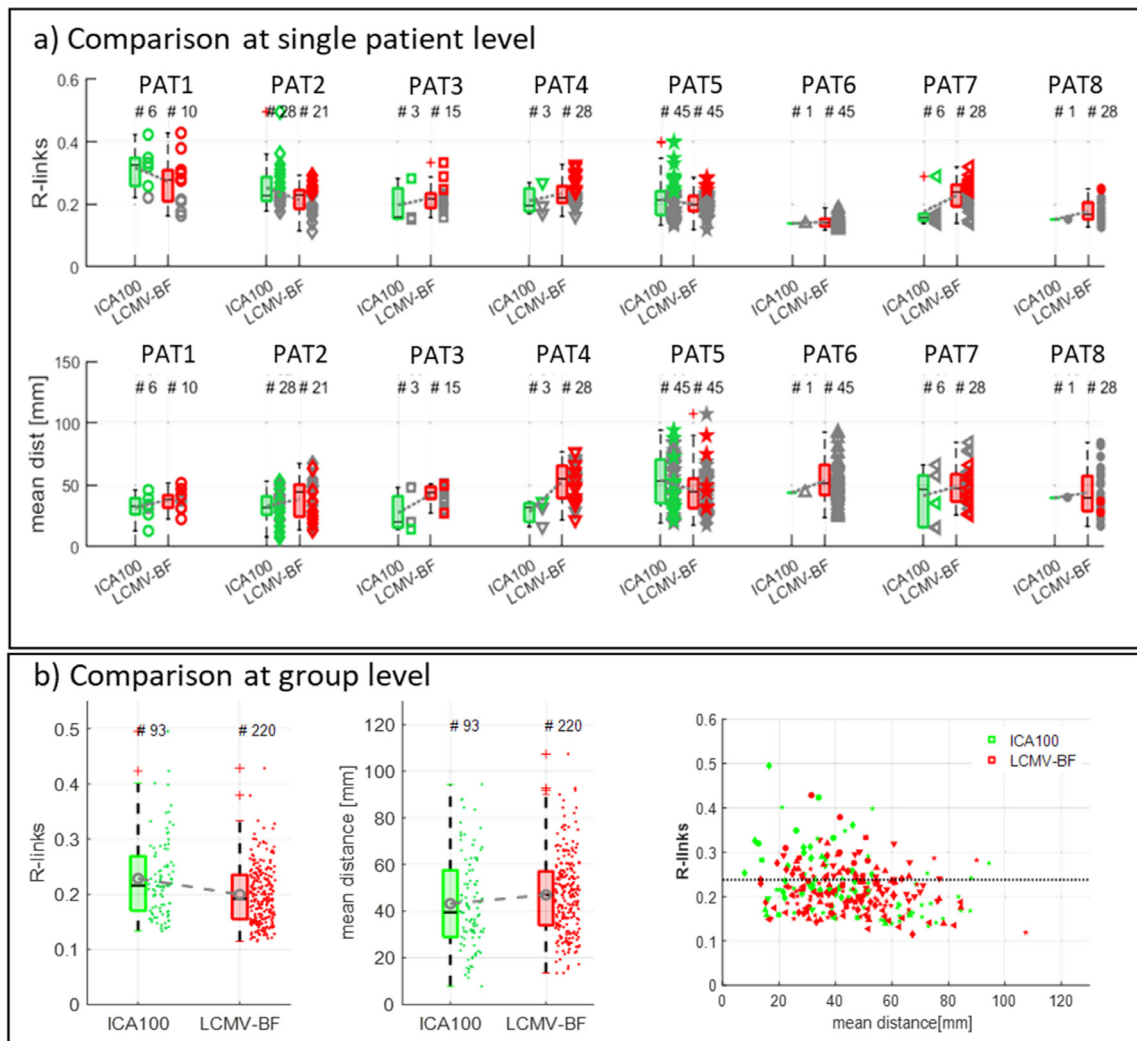


Fig. 7. Real data results on the link dynamics. a) Top: comparison of maximum correlation values between each MEG link and SEEG links among the two considered methods separately for single patients. Bottom: respective mean distances between nodes of the correlated links. Gray markers identify under threshold R values and the associated distances. Gray lines connect the distribution means. The number of ICs and LCMV-BFs links is reported above. b) Left: boxplots comparing the correlation coefficients between links. Middle: mean of the two distances between nodes for all the patients together. Right: scatterplots of the R values between inside/outside links as a function of the sum of the distances. Different markers represent different patients, accordingly to panel a), the dashed line indicates the LFDR threshold across all the R values.

Hall et al., 2018; Jiang et al., 2022; Kirsch et al., 2006; Malinowska et al., 2014; Velmurugan et al., 2018).

In the present work, we further validated the possibility to retrieve the epileptic network (EN) organization from MEG data and, for the first time to the best of our knowledge, we compared and validated ICA and LCMV beamformer in the computation of dynamic connectivity through

simulations, and against simultaneously recorded SEEG data in 8 epileptic patients.

Our first simulation (SIM1) demonstrated that both methods can adequately retrieve the simulated source activities, but with different effect of the temporal correlation and spatial configuration among sources (Fig. 3). It emerged that, even if ICA (both ICA 50 and ICA 100) was

more affected by high temporal correlation, the overall $QofR$ was significantly higher in the case of ICA100 than LCMV-BF and ICA50. This result indicated that ICA reconstructs the activity more accurately in most conditions. Indeed, previous studies also showed that ICA was able to retrieve interictal sources maintaining the spike and wave morphology (Kobayashi et al., 1999; Matsubara et al., 2020). This result was also related to the higher impact of the cross-talk phenomenon (leakage) on the LCMV-BF reconstructed time series (Fig. 3d). Conversely, the localization performances were significantly superior for the LCMV-BF in term of $QofL$, an index based on the localization error. Such an outcome pointed out the already discussed difficulties in localizing non perfectly dipolar ICA topographies (Malinowska et al., 2014), and the reliability of the beamformer technique in detecting and localizing multiple sources without prior knowledge on their number (Kirsch et al., 2006; Van Veen et al., 1997). Beamformer was also robust, up to a certain level, against temporal correlation with little source distortion (Sekihara et al., 2002). Of note, in this work, we decided to proceed with the single dipole fitting method to localize ICs compare the results across methods, both on simulated and real data. This way, a single source was associated to each selected time series (ICs and virtual electrode signals). Another reason supporting this choice was the intention of performing a dynamic connectivity analysis on the extracted components and LCMV sources as they are localized in different positions. Still, multiple sources could be fitted to the ICA topographies, in cases where level of correlation is high (Benar et al., 2005; Sorrentino et al., 2014).

In our study, the term ‘dynamic’ refers to the application of a connectivity index (broadband cross-correlation) using a short sliding window along the continuous data. As already discussed in (Malinowska et al., 2014), to perform connectivity analysis on ICs may sound contradictory because of the independency constraint that is intrinsic in the ICA algorithm. In our case, the network we wanted to identify was the interictal one, that manifests itself during IED, thus we assumed that the spikes interaction and propagation can be detected with cross-correlation, which can capture propagation lags. Of note, we also showed that ICA can correctly separate correlated sources, with a correlation value up to 0.8 (Fig. 3a), thus the independence constraint seems not to strongly affect source separation. In SIM2, we simulated an interictal network with three nodes and a connectivity pattern only based on the delay between the co-occurring events. We tested the possibility to retrieve such network dynamic using cross-correlation on both the simulated and reconstructed time series (i.e., selected ICs and LCMV-BF virtual electrodes), and correlating the time course of each link between nodes. We mainly used this simulation as a proof of concept to test whether the retrieval was possible and, in the used time and spatial configurations, ICA showed better performance in terms of SIM/MEG links time course correlation.

Encouraging results were also obtained by applying the same pipeline to real data of eight drug-resistant epileptic patients who underwent a simultaneous SEEG/MEG recording. We excluded the ICA50 approach since ICA100 showed better results on simulated data, probably due to the higher percentage of original data variance retained (Artoni et al., 2018). Indeed, the need of maintaining as much as possible the full rank of the data has been suggested for a 69 channels EEG dataset, even if, stereotyped sources (as we can consider the IED sources) seem not to be degraded by the application of the PCA before ICs decomposition (Artoni et al., 2018).

With an approach similar to the one adopted in previous studies (Fahimi Hnazaee et al., 2020; Pizzo et al., 2019), we first extracted, for each identified interictal source, the mostly correlated (Pearson’s correlation coefficient) bipolar SEEG channel, and then computed the Euclidean distance between the SEEG channel position and the localized source. Since for each patient a different number of ICs and LCMV-BF sources were identified as potentially interictal, and because of the large intra- and inter-patient variability, in the statistical test at the group level we took in consideration the random effect due to patient individual characteristics. The absence of any significant difference showed

that, on average, the approaches performed equally well. However, the performance changed patient by patient: at the single case level, no method was evidently superior to the other. An advantage of ICA is that it reduces drastically the dimension of the problem, leading to a more straightforward interpretation.

We found that, in 6 out of 8 patients, at least one significant correlation was present ($|R| > 0.34$) and in 4 of them ICA showed a better trade-off between correlation and estimated distance. What we already pointed out on the simulations about the difficult localization of the ICs when their topography is not dipolar, was also seen in real data. As suggested by the already mentioned work (Malinowska et al., 2014), a complex spatial pattern could already identify a network activity, being the summation of different interictal sources interacting almost synchronously, so that, because of its limitation, ICA is unable to properly separate them (Makeig et al., 2004). If the complex spatial pattern can be separated, for example with multi-dipole localization (Viani et al., 2020), such complex topographies would already indicate a strong network connectivity between the underlying sources – in a static way though.

The retrieval of the dynamic of network links was also possible, but the interpretation is less straightforward. For simplicity we only indicated the mostly correlated SEEG network link for each MEG-based network link. In two patients, LCMV-BF revealed significant correspondences with medium correlation values for several network links, while only one significance was present for IC based networks. In patient 1, 2, 3 and 5 equally good outcome was found, with both close correlation values and distances. Therefore, we cannot identify a clear ‘winning’ method, but instead our results suggest that both methods provide useful information that could be used in combination. In this line, an interesting venue is to perform ICA on the beamformer ‘virtual sources’, which could benefit of the complementary advantages of the two methods (Velmurugan et al., 2022).

4.1. Limitations of the study and future perspectives

With the intention of carrying out a comparison of methods as fair as possible, some methodological limitations were introduced in this work, and we want to discuss them providing suggestions for future research and improvements.

As already discussed, dipole localization can be considered a sub-optimal method to localize ICs with complex topography, and at the same time, the choice of only considering the local maxima of the beamformer kurtosis also is a simplification. Even though, such simplifications were considered necessary to perform a direct association with the SEEG setup (and simulations), since our analysis was principally methodological. In order to investigate the clinical validity of our results, further analyses are needed, including the use of more sophisticated forward models (i.e., higher spatial resolution, and BEM), multi-dipoles ICs localization and beamformers source-leakage correction and mapping to specific atlas, i.e. the Virtual Epileptic Patient-VEP atlas (Wang et al., 2021).

In this study, we exploited the IED as a reference of interictal activity because in many cases it is clearly discernible on MEG signals and sources time series. Since interictal activity may be generated by complex networks (Badier and Chauvel, 1995; Lagarde et al., 2018), the involved brain regions may not be properly sampled by the SEEG contacts. Indeed, even if simultaneous SEEG recording represents a trustable ‘ground truth’ in controlled conditions (Mikulan et al., 2020), it could be considered imperfect in complex pathological states. Nevertheless, it still provides the best validation option for spontaneous activity, given accurate pre-implantation evaluations. Therefore, identification of an interictal source far from the correlated SEEG contact, but still in regions sampled by SEEG, was here interpreted as a ‘bad’ outcome.

In this direction, simultaneous MEG/SEEG recordings are undoubtedly a step forward to a more precise EN characterization because the MEG provide a whole brain view to the activity locally recorded

invasively (Badier et al., 2017; Vivekananda et al., 2021), possibly reducing the number of missed IED sources (Gavaret et al., 2016).

As for the connectivity analysis performed in this study, we decided to apply a linear cross-correlation analysis and dynamically track the evolution of each network link along the whole recording with a 1-sec time resolution. We showed that it is possible to identify which SEEG/MEG links evolve in a similar way, possibly opening the way to the analysis of much more complex interactions between the MEG and SEEG networks, which has been done so far in a static manner (Malinowska et al., 2014). Possible improvements will comprise the application of non-linear connectivity indexes such as H2 (Courtenes et al., 2016). The idea is that it would be possible to retrieve, using MEG, the on/off dynamic of the EN and possibly model its dynamic connectivity as done, for example, for physiological networks (Battaglia and Brovelli, 2019).

5. Conclusion

We presented a first comparison of two approaches for estimating IED activity and their dynamic connectivity non-invasively from MEG data, namely independent component analysis (ICA) and linearly constrained minimum-variance beamformer (LCMV-BF). We conclude, after a simulation study and a test with SEEG data recorded simultaneously in 8 epileptic patients, that the two methods are comparable in performance and complementary in identifying the sources of interictal activity. Specifically, ICA reconstructed the sources more accurately in terms of time series activity than the LCMV-BF, but it was inferior in term of localization on simulated data. On real simultaneous MEG/SEEG recordings, results showed an overall better performance of the ICA (i.e., higher time series correlation, lower distance between the source estimated position and correlated SEEG contact). On a patient by patient bases, it could be suggested that when the sources of interictal activity are independent, even if relatively close in space, ICA can better separate and capture their dynamics and interactions in an easily interpretable way. Conversely, when the sources are more correlated (Fig. S3), ICA tends to merge them, while the LCMV-BF, being itself distributed, can identify more sources simultaneously. In this latter case, LCMV may need additional post-processing for a better interpretation and source leakage correction (Brookes et al., 2012). We further demonstrated the possibility of using ICA and LCMV-BF to retrieve the EN dynamic non-invasively. While in the simulated study ICA performed clearly better, on real data the two methods showed equivalent results. This may open to the possibility of better understanding how different epileptic sources dynamically interacts, thus fully exploiting non-invasive whole brain information.

Data and code availability statements

MEG, intracranial data and MRI images cannot be shared due to restrictions on patient data from APHM. The simulated data and analysis scripts are available upon reasonable request from the corresponding author. AnyWave software, used for cross-correlation analysis, is freely available at <https://ins-amu.fr/software>.

Declaration of Competing Interest

The authors declare no competing financial interests.

Credit authorship contribution statement

Stefania Coelli: Methodology, Software, Formal analysis, Visualization, Writing – original draft, Writing – review & editing. **Samuel Medina Villalon:** Software, Methodology, Data curation, Writing – original draft, Writing – review & editing. **Francesca Bonini:** Investigation, Validation, Writing – review & editing. **Jayabal Velmurugan:** Software,

Writing – original draft, Writing – review & editing. **Víctor J. López-Madrona:** Software, Writing – original draft, Writing – review & editing. **Romain Carron:** Investigation, Writing – review & editing. **Fabrice Bartolomei:** Resources, Supervision, Funding acquisition. **Jean-Michel Badier:** Conceptualization, Methodology, Data curation, Funding acquisition, Supervision. **Christian-G. Bénar:** Conceptualization, Resources, Methodology, Writing – review & editing, Supervision, Funding acquisition, Project administration.

Data Availability

The data that has been used is confidential.

Acknowledgements

S.C. was founded by Fondazione CRUI (GO for IT program), Italy.

This research was also supported by grants ANR-16-CONV-0002 (ILCB), ANR-17-HBPR-0005 (SCALES) from Agence Nationale de la recherche and, A*MIDEX project ANR-17-RHUS-0004 (EPINOV) funded by the ‘Investissements d’Avenir’ managed by the French National Research Agency. This work has received support from the French government under the Programme « Investissements d’Avenir », Initiative d’Excellence d’Aix-Marseille Université via A*Midex funding (AMX-19-IET-004), and ANR (ANR-17-EURE-0029). It was performed on a platform member of France Life Imaging network (grant ANR-11-INBS-0006).

Supplementary materials

Supplementary material associated with this article can be found, in the online version, at doi:[10.1016/j.neuroimage.2022.119806](https://doi.org/10.1016/j.neuroimage.2022.119806).

References

- Artoni, F., Delorme, A., Makeig, S., 2018. Applying dimension reduction to EEG data by principal component analysis reduces the quality of its subsequent independent component decomposition. *Neuroimage* 175, 176–187. doi:[10.1016/j.neuroimage.2018.03.016](https://doi.org/10.1016/j.neuroimage.2018.03.016).
- Badier, J., Chauvel, P., 1995. Spatio-temporal characteristics of paroxysmal interictal events in human temporal lobe epilepsy. *J. Physiol.* 89, 255–264. doi:[10.1016/0928-4257\(96\)83642-4](https://doi.org/10.1016/0928-4257(96)83642-4).
- Badier, J.M., Dubarry, A.S., Gavaret, M., Chen, S., Trébuchon, A.S., Marquis, P., Régis, J., Bartolomei, F., Bénar, C.G., Carron, R., 2017. Technical solutions for simultaneous MEG and SEEG recordings: towards routine clinical use. *Physiol. Meas.* 38, N118–N127. doi:[10.1088/1361-6579/aa7655](https://doi.org/10.1088/1361-6579/aa7655).
- Baillet, S., 2017. Magnetoencephalography for brain electrophysiology and imaging. *Nat. Neurosci.* 20, 327–339. doi:[10.1038/nn.4504](https://doi.org/10.1038/nn.4504).
- Barborica, A., Mindruta, I., Sheybani, L., Spinelli, L., Oane, I., Pistol, C., Donos, C., López-Madrona, V.J., Vulliamoz, S., Bénar, C.-G., 2021. Extracting seizure onset from surface EEG with independent component analysis: insights from simultaneous scalp and intracerebral EEG. *NeuroImage Clin.* 32, 102838. doi:[10.1016/j.nicl.2021.102838](https://doi.org/10.1016/j.nicl.2021.102838).
- Bartolomei, F., Lagarde, S., Wendling, F., McGonigal, A., Jirsa, V., Guye, M., Bénar, C., 2017. Defining epileptogenic networks: contribution of SEEG and signal analysis. *Epilepsia* 58, 1131–1147. doi:[10.1111/epi.13791](https://doi.org/10.1111/epi.13791).
- Battaglia, D., Brovelli, A., 2019. Functional connectivity and neuronal dynamics : insights from computational methods. *Cogn. Neurosci.*
- Bell, A.J., Sejnowski, T.J., 1995. An information-maximization approach to blind separation and blind deconvolution. *Neural Comput* 7, 1129–1159. doi:[10.1162/neco.1995.7.6.1129](https://doi.org/10.1162/neco.1995.7.6.1129).
- Bénar, C.-G., Gunn, R.N., Grova, C., Champagne, B., Gotman, J., 2005. Statistical maps for EEG dipolar source localization. *IEEE Trans. Biomed. Eng.* 52, 401–413. doi:[10.1109/TBME.2004.841263](https://doi.org/10.1109/TBME.2004.841263).
- Benjamini, Y., Heller, R., 2007. False discovery rates for spatial signals. *J. Am. Stat. Assoc.* doi:[10.1198/016214507000000941](https://doi.org/10.1198/016214507000000941).
- Bouet, R., Jung, J., Delpuech, C., Ryvlin, P., Isnard, J., Guenet, M., Bertrand, O., Mauguière, F., 2012. Towards source volume estimation of interictal spikes in focal epilepsy using magnetoencephalography. *Neuroimage* 59, 3955–3966. doi:[10.1016/j.neuroimage.2011.10.052](https://doi.org/10.1016/j.neuroimage.2011.10.052).
- Brookes, M.J., Woolrich, M.W., Barnes, G.R., 2012. Measuring functional connectivity in MEG: a multivariate approach insensitive to linear source leakage. *Neuroimage* 63, 910–920. doi:[10.1016/j.neuroimage.2012.03.048](https://doi.org/10.1016/j.neuroimage.2012.03.048).
- Colombet, B., Woodman, M., Badier, J.M., Bénar, C.G., 2015. AnyWave: a cross-platform and modular software for visualizing and processing electrophysiological signals. *J. Neurosci. Methods* 242, 118–126. doi:[10.1016/j.jneumeth.2015.01.017](https://doi.org/10.1016/j.jneumeth.2015.01.017).
- Colton, D., Kress, R., 1992. *Electromagnetic Scattering Theory*. Springer, Berlin New Edition. Ed.

- Comon, P., 1994. Independent component analysis, a new concept? *Signal Process.* 36, 287–314. doi:[10.1016/0165-1684\(94\)90029-9](https://doi.org/10.1016/0165-1684(94)90029-9).
- Courtsens, S., Colombet, B., Trébuchon, A., Brovelli, A., Bartolomei, F., Bénar, C.G., 2016. Graph measures of node strength for characterizing preictal synchrony in partial epilepsy. *Brain Connect* 6, 530–539. doi:[10.1089/brain.2015.0397](https://doi.org/10.1089/brain.2015.0397).
- Fahimi Hnazeae, M., Wittevrongel, B., Khachatryan, E., Libert, A., Carrette, E., Dauwe, I., Meurs, A., Boon, P., Van Roost, D., Van Hulle, M.M., 2020. Localization of deep brain activity with scalp and subdural EEG. *Neuroimage* 223, 117344. doi:[10.1016/j.neuroimage.2020.117344](https://doi.org/10.1016/j.neuroimage.2020.117344).
- Gavaret, M., Dubarry, A.-S., Carron, R., Bartolomei, F., Trébuchon, A., Bénar, C.-G., 2016. Simultaneous SEEG-MEG-EEG recordings overcome the SEEG limited spatial sampling. *Epilepsy Res* 128, 68–72. doi:[10.1016/j.epilepsyres.2016.10.013](https://doi.org/10.1016/j.epilepsyres.2016.10.013).
- Grova, C., Aiguabella, M., Zelmann, R., Lina, J.-M., Hall, J.A., Kobayashi, E., 2016. Intracranial EEG potentials estimated from MEG sources: a new approach to correlate MEG and iEEG data in epilepsy. *Hum. Brain Mapp.* 37, 1661–1683. doi:[10.1002/hbm.23127](https://doi.org/10.1002/hbm.23127).
- Grova, C., Daunizeau, J., Lina, J.M., Bénar, C.G., Benali, H., Gotman, J., 2006. Evaluation of EEG localization methods using realistic simulations of interictal spikes. *Neuroimage* 29, 734–753. doi:[10.1016/j.neuroimage.2005.08.053](https://doi.org/10.1016/j.neuroimage.2005.08.053).
- Hall, M.B.H., Nissen, I.A., van Straaten, E.C.W., Furlong, P.L., Witton, C., Foley, E., Seri, S., Hillebrand, A., 2018. An evaluation of kurtosis beamforming in magnetoencephalography to localize the epileptogenic zone in drug resistant epilepsy patients. *Clin. Neurophysiol.* 129, 1221–1229. doi:[10.1016/j.clinph.2017.12.040](https://doi.org/10.1016/j.clinph.2017.12.040).
- Hassan, M., Merlet, I., Mheich, A., Kabbara, A., Biraben, A., Nica, A., Wendling, F., 2017. Identification of interictal epileptic networks from dense-EEG. *Brain Topogr.* 30, 60–76. doi:[10.1007/s10548-016-0517-z](https://doi.org/10.1007/s10548-016-0517-z).
- He, B., Astolfi, L., Valdes-Sosa, P.A., Marinazzo, D., Palva, S.O., Benar, C.G., Michel, C.M., Koenig, T., 2019. Electrophysiological brain connectivity: theory and implementation. *IEEE Trans. Biomed. Eng.* 66, 2115–2137. doi:[10.1109/TBME.2019.2913928](https://doi.org/10.1109/TBME.2019.2913928).
- Hillebrand, A., Nissen, I.A., Ris-Hilgersom, I., Sijms, N.C.G., Ronner, H.E., van Dijk, B.W., Stam, C.J., 2016. Detecting epileptiform activity from deeper brain regions in spatially filtered MEG data. *Clin. Neurophysiol.* 127, 2766–2769. doi:[10.1016/j.clinph.2016.05.272](https://doi.org/10.1016/j.clinph.2016.05.272).
- Jaiswal, A., Nenonen, J., Stenroos, M., Gramfort, A., Dalal, S.S., Westner, B.U., Litvak, V., Mosher, J.C., Schoffelen, J.M., Witton, C., Oostenveld, R., Parkkonen, L., 2020. Comparison of beamformer implementations for MEG source localization. *Neuroimage* 216. doi:[10.1016/j.neuroimage.2020.116797](https://doi.org/10.1016/j.neuroimage.2020.116797).
- Jiang, X., Ye, S., Sohrabpour, A., Bagić, A., He, B., 2022. Imaging the extent and location of spatiotemporally distributed epileptiform sources from MEG measurements. *NeuroImage Clin.* 33, 102903. doi:[10.1016/j.nicl.2021.102903](https://doi.org/10.1016/j.nicl.2021.102903).
- Jmail, N., Gavaret, M., Bartolomei, F., Chauvel, P., Badier, J.-M., Bénar, C.-G., 2016. Comparison of Brain Networks During Interictal Oscillations and Spikes on Magnetoencephalography and Intracerebral EEG. *Brain Topogr.* 29, 752–765. doi:[10.1007/s10548-016-0501-7](https://doi.org/10.1007/s10548-016-0501-7).
- Kirsch, H.E., Robinson, S.E., Mantle, M., Nagarajan, S., 2006. Automated localization of magnetoencephalographic interictal spikes by adaptive spatial filtering. *Clin. Neurophysiol.* 117, 2264–2271. doi:[10.1016/j.clinph.2006.06.708](https://doi.org/10.1016/j.clinph.2006.06.708).
- Kobayashi, K., Akiyama, T., Nakahori, T., Yoshinaga, H., Ohtsuka, Y., Gotman, J., Oka, E., 2002. Source estimation of spikes by a combination of independent component analysis and RAP-MUSIC. *Int. Congr. Ser.* 1232, 311–316. doi:[10.1016/S0531-5131\(01\)00713-0](https://doi.org/10.1016/S0531-5131(01)00713-0).
- Kobayashi, K., James, C.J., Nakahori, T., Akiyama, T., Gotman, J., 1999. Isolation of epileptiform discharges from unaveraged EEG by independent component analysis. *Clin. Neurophysiol.* 110, 1755–1763. doi:[10.1016/S1388-2457\(99\)00134-0](https://doi.org/10.1016/S1388-2457(99)00134-0).
- Kobayashi, K., Merlet, I., Gotman, J., 2001. Separation of spikes from background by independent component analysis with dipole modeling and comparison to intracranial recording. *Clin. Neurophysiol.* 112, 405–413. doi:[10.1016/S1388-2457\(01\)00457-6](https://doi.org/10.1016/S1388-2457(01)00457-6).
- Lagarde, S., Roehri, N., Lambert, I., Trebuchon, A., McGonigal, A., Carron, R., Scavarda, D., Milh, M., Pizzo, F., Colombet, B., Giusiano, B., Medina Villalon, S., Guye, M., Bénar, C.G., Bartolomei, F., 2018. Interictal stereotactic-EEG functional connectivity in refractory focal epilepsies. *Brain* 141, 2966–2980. doi:[10.1093/brain/awy214](https://doi.org/10.1093/brain/awy214).
- Lamus, C., Hämäläinen, M.S., Temereanca, S., Brown, E.N., Purdon, P.L., 2012. A spatiotemporal dynamic distributed solution to the MEG inverse problem. *Neuroimage* 63, 894–909. doi:[10.1016/j.neuroimage.2011.11.020](https://doi.org/10.1016/j.neuroimage.2011.11.020).
- Li, R., Plummer, C., Vogrin, S.J., Woods, W.P., Kuhlmann, L., Boston, R., Liley, D.T.J., Cook, M.J., Grayden, D.B., 2021. Interictal spike localization for epilepsy surgery using magnetoencephalography beamforming. *Clin. Neurophysiol.* 132, 928–937. doi:[10.1016/j.clinph.2020.12.019](https://doi.org/10.1016/j.clinph.2020.12.019).
- Lin, Y.Y., Shih, Y.H., Hsieh, J.C., Yu, H.Y., Yiu, C.H., Wong, T.T., Yeh, T.C., Kwan, S.Y., Ho, L.T., Yen, D.J., Wu, Z.A., Chang, M.S., 2003. Magnetoencephalographic yield of interictal spikes in temporal lobe epilepsy: comparison with scalp EEG recordings. *Neuroimage* 19, 1115–1126. doi:[10.1016/S1053-8119\(03\)00181-2](https://doi.org/10.1016/S1053-8119(03)00181-2).
- López-Madróna, V.J., Medina Villalon, S., Badier, J., Trébuchon, A., Jayabal, V., Bartolomei, F., Carron, R., Barborica, A., Vulliémoz, S., Alario, F.X., Bénar, C.G., 2022. Magnetoencephalography can reveal deep brain network activities linked to memory processes. *Hum. Brain Mapp.* doi:[10.1002/hbm.25987](https://doi.org/10.1002/hbm.25987).
- Makeig, S., Debener, S., Onton, J., Delorme, A., 2004. Mining event-related brain dynamics. *Trends Cogn. Sci.* 8, 204–210. doi:[10.1016/j.tics.2004.03.008](https://doi.org/10.1016/j.tics.2004.03.008).
- Malinowska, U., Badier, J.-M., Gavaret, M., Bartolomei, F., Chauvel, P., Bénar, C.-G., 2014. Interictal networks in Magnetoencephalography. *Hum. Brain Mapp.* 35, 2789–2805. doi:[10.1002/hbm.22367](https://doi.org/10.1002/hbm.22367).
- Matsubara, T., Hironaga, N., Uehara, T., Chatani, H., Tobimatsu, S., Kishida, K., 2020. A novel method for extracting interictal epileptiform discharges in multi-channel MEG: use of fractional type of blind source separation. *Clin. Neurophysiol.* 131, 425–436. doi:[10.1016/j.clinph.2019.11.032](https://doi.org/10.1016/j.clinph.2019.11.032).
- Medina Villalon, S., Paz, R., Roehri, N., Lagarde, S., Pizzo, F., Colombet, B., Bartolomei, F., Carron, R., Bénar, C.G., 2018. EpiTools, a software suite for presurgical brain mapping in epilepsy: intracerebral EEG. *J. Neurosci. Methods* 303, 7–15. doi:[10.1016/j.jneumeth.2018.03.018](https://doi.org/10.1016/j.jneumeth.2018.03.018).
- Merlet, I., Gotman, J., 1999. Reliability of dipole models of epileptic spikes. *Clin. Neurophysiol.* 110, 1013–1028. doi:[10.1016/S1388-2457\(98\)00062-5](https://doi.org/10.1016/S1388-2457(98)00062-5).
- Mikulan, E., Russo, S., Parmigiani, S., Sarasso, S., Zauli, F.M., Rubino, A., Avanzini, P., Cattani, A., Sorrentino, A., Gibbs, S., Cardinale, F., Sartori, L., Nobili, L., Massimini, M., Pigorini, A., 2020. Simultaneous human intracerebral stimulation and HD-EEG, ground-truth for source localization methods. *Sci. Data* 7, 1–8. doi:[10.1038/s41597-020-0467-x](https://doi.org/10.1038/s41597-020-0467-x).
- Oostenveld, R., Fries, P., Maris, E., Schoffelen, J.-M., 2011. FieldTrip: open source software for advanced analysis of MEG, EEG, and invasive electrophysiological data. *Comput. Intell. Neurosci.* 2011, 1–9. doi:[10.1155/2011/156869](https://doi.org/10.1155/2011/156869).
- Ossadtdchi, A., Baillet, S., Mosher, J.C., Thyerlei, D., Sutherling, W., Leahy, R.M., 2004. Automated interictal spike detection and source localization in magnetoencephalography using independent components analysis and spatio-temporal clustering. *Clin. Neurophysiol.* 115, 508–522. doi:[10.1016/j.clinph.2003.10.036](https://doi.org/10.1016/j.clinph.2003.10.036).
- Pizzo, F., Roehri, N., Medina Villalon, S., Trébuchon, A., Chen, S., Lagarde, S., Carron, R., Gavaret, M., Giusiano, B., McGonigal, A., Bartolomei, F., Badier, J.M., Bénar, C.G., 2019. Deep brain activities can be detected with magnetoencephalography. *Nat. Commun.* 10, 971. doi:[10.1038/s41467-019-08665-5](https://doi.org/10.1038/s41467-019-08665-5).
- Roehri, N., Lina, J.M., Mosher, J.C., Bartolomei, F., Benar, C.G., 2016. Time-frequency strategies for increasing high-frequency oscillation detectability in intracerebral EEG. *IEEE Trans. Biomed. Eng.* 63, 2595–2606. doi:[10.1109/TBME.2016.2556425](https://doi.org/10.1109/TBME.2016.2556425).
- Roehri, N., Pizzo, F., Bartolomei, F., Wendling, F., Bénar, C.G., 2017. What are the assets and weaknesses of HFO detectors? A benchmark framework based on realistic simulations. *PLoS ONE* 12, 1–20. doi:[10.1371/journal.pone.0174702](https://doi.org/10.1371/journal.pone.0174702).
- Sekihara, K., Nagarajan, S.S., Poeppel, D., Marantz, A., 2002. Performance of an MEG adaptive-beamformer technique in the presence of correlated neural activities: effects on signal intensity and time-course estimates. *IEEE Trans. Biomed. Eng.* 49, 1534–1546. doi:[10.1109/TBME.2002.805485](https://doi.org/10.1109/TBME.2002.805485).
- Sorrentino, A., Luria, G., Aramini, R., 2014. Bayesian multi-dipole modelling of a single topography in MEG by adaptive sequential Monte Carlo samplers. *Inverse Probl.* 30, 045010. doi:[10.1088/0266-5611/30/4/045010](https://doi.org/10.1088/0266-5611/30/4/045010).
- Tadel, F., Baillet, S., Mosher, J.C., Pantazis, D., Leahy, R.M., 2011. Brainstorm: a user-friendly application for MEG/EEG analysis. *Comput. Intell. Neurosci.* 2011, 1–13. doi:[10.1155/2011/879716](https://doi.org/10.1155/2011/879716).
- Van Veen, B.D., Van Drongelen, W., Yuchtman, M., Suzuki, A., 1997. Localization of brain electrical activity via linearly constrained minimum variance spatial filtering. *IEEE Trans. Biomed. Eng.* 44, 867–880. doi:[10.1109/10.623056](https://doi.org/10.1109/10.623056).
- Velmurugan, J., Badier, J.M., Pizzo, F., Villalon, S.M., Papageorgakis, C., López-Madróna, V., Jegou, A., Carron, R., Bartolomei, F., Bénar, C.-G., 2022. Virtual MEG sensors based on beamformer and independent component analysis can reconstruct epileptic activity as measured on simultaneous intracerebral recordings. *Neuroimage* 119681. doi:[10.1016/j.neuroimage.2022.119681](https://doi.org/10.1016/j.neuroimage.2022.119681).
- Velmurugan, J., Nagarajan, S.S., Mariyappa, N., Ravi, S.G., Thennarasu, K., Mundluri, R.C., Raghavendra, K., Bharath, R.D., Saini, J., Arivazhagan, A., Rajan, J., Mahadevan, A., Rao, M.B., Satishchandra, P., Sinha, S., 2018. Magnetoencephalographic imaging of ictal high-frequency oscillations (80–200 Hz) in pharmacologically resistant focal epilepsy. *Epilepsia* 59, 190–202. doi:[10.1111/epi.13940](https://doi.org/10.1111/epi.13940).
- Viani, A., Luria, G., Bornfleth, H., Sorrentino, A., 2020. Where Bayes tweaks Gauss: conditionally Gaussian priors for stable multi-dipole estimation. arXiv:[2006.04141v1](https://arxiv.org/abs/2006.04141v1).
- Vivekananda, U., Cao, C., Liu, W., Zhang, J., Rugg-Gunn, F., Walker, M.C., Litvak, V., Sun, B., Zhan, S., 2021. The use of simultaneous stereo-electroencephalography and magnetoencephalography in localizing the epileptogenic focus in refractory focal epilepsy. *Brain Commun* 3, 1–9. doi:[10.1093/braincomms/fcab072](https://doi.org/10.1093/braincomms/fcab072).
- Wang, H.E., Scholly, J., Triebkorn, P., Sip, V., Medina Villalon, S., Woodman, M.M., Le Troter, A., Guye, M., Bartolomei, F., Jirsa, V., 2021. VEP atlas: an anatomic and functional human brain atlas dedicated to epilepsy patients. *J. Neurosci. Methods* 348, 108983. doi:[10.1016/j.jneumeth.2020.108983](https://doi.org/10.1016/j.jneumeth.2020.108983).
- Wilenius, J., Lauronen, L., Kirveskari, E., Gaily, E., Metsähonkala, L., Paetau, R., 2020. Interictal magnetoencephalography in parietal lobe epilepsy – Comparison of equivalent current dipole and beamformer (SAMepi) analysis. *Clin. Neurophysiol. Pract.* 5, 64–72. doi:[10.1016/j.cnp.2020.02.003](https://doi.org/10.1016/j.cnp.2020.02.003).